PAPER • **OPEN ACCESS**

Revisiting contact potential difference in electrostatic force microscopy

To cite this article: Lukas Lehnert *et al* 2026 *J. Phys. Commun.* **10** 015007

Journal of Physics Communications

OPEN ACCESS

RECEIVED
22 August 2025

REVISED
10 December 2025

ACCEPTED FOR PUBLICATION
24 December 2025

PUBLISHED
2 February 2026

PAPER

Revisiting contact potential difference in electrostatic force microscopy

Lukas Lehnert[1], **Ronald Thoelen**[2] and **Hildegard Möbius**[1,*]

[1] Department of Computer Sciences/Micro Systems Technology, University of Applied Sciences Kaiserslautern, Zweibrücken, Germany
[2] Institute for Materials Research, Hasselt University, Hasselt, Belgium
[*] Author to whom any correspondence should be addressed.

E-mail: hildegard.moebius@hs-kl.de

Keywords: electrostatic force microscopy, contact potential difference, tip-substrate interaction, nanoparticles, magnetic force microscopy, kelvin probe force microscopy

Supplementary material for this article is available online

Abstract

Understanding the tip–substrate interaction in Electrostatic Force Microscopy (EFM) is essential for the quantitative analysis of experimental data. In this work, the role of the contact potential difference (V_{CPD}) between tip and substrate, both experimentally and theoretically, is investigated. Over the past decades, several models have been proposed to describe the tip–substrate interaction, commonly assuming an equipotential surface on the tip. A common feature of these models is the treatment of V_{CPD} as an additional voltage, which is added to the externally applied voltage V_{DC}. In EFM a non-zero vertex of the voltage parabola is reported in several publications which cannot be explained by theory so far. We investigate experimentally if a model with different contributions for cone and apex better explains experimental data.

1. Introduction

Atomic Force Microscopy (AFM) based methods such as Magnetic Force Microscopy (MFM), Kelvin Probe Force Microcopy (KPFM) and Electrostatic Force Microscopy (EFM) have been developed to powerful tools to monitor electric and magnetic properties as well as the contact potential difference (V_{CPD}) on a microscopic scale with lateral resolution in the nanometer range. Particularly, the non-contact modes allow the determination of long-range forces such as electrostatic and magnetic forces by separating them from the short-range forces through the distance to the sample.

In MFM a magnetized tip is used to image magnetic domains, structures on surfaces and even to map magnetic signals of single nanoparticles [1–4]. KPFM is used to locally map the work function for metals or charge distributions for isolators [5–7]. EFM, characterized by applying a voltage between tip and sample, has been proven as a suitable tool to gain electrostatic information such as charge distribution and dielectric constants of thin film dielectric layers and nanoparticles for a wide range of applications [8, 9]. Motivated by semiconductor industry as well as by biomedical applications quantitative measurements of dielectric properties of films with thicknesses in the nanometer range with nanometer lateral resolution has become an important topic in research [10–13]. Gramse *et al* presented a method based on standard DC voltage EFM which allows the determination of thin film dielectric constants with any commercial atomic force microscope [14]. Fumagalli *et al* succeeded in the determination of the dielectric constant of nanoparticles by combining EFM data with precise numerical simulation of the tip-sample interaction [15]. All three methods use non-contact mode by moving an oscillating tip a distance z, called lift-height, away from the sample. In this arrangement tip and substrate form a capacitor depending on the contact potential difference V_{CPD}, the applied voltage V_{DC} and the shape of the tip. The phase (Φ), between the excitation signal and the measured oscillation of the cantilever, is proportional to the second derivative of the tip-substrate capacitance. In MFM there is no externally applied voltage. Thus, the phase shift corresponds to zero voltage measurements in EFM when no magnetic material is

present. In MFM the only voltage inducing a capacitive coupling effect is V_{CPD}. In KPFM an applied voltage is used to compensate V_{CPD} in order to determine V_{CPD}. Therefore, V_{CPD} and the shape of the tip are the common parameters of relevance in MFM, KPFM and EFM.

There exist two main approaches to describe and analyze the tip-substrate interaction as a function of lift-height z: analytical approaches that divide the tip into apex, cone and cantilever to model the interaction with the sample [16–21], and complex 3D-Finite Element Methods (FEM) simulations [15, 22, 23]. The analytical models distinguish between z-dependency contributions of apex, cone and cantilever. Experiments reveal that for distances smaller than the tip radius the apex dominates the interaction whereas for distances larger than the tip radius the cone contribution becomes relevant [16–18]. FEM simulations require the solution of Poisson's equation leading to a charge distribution on the tip surface for an equipotential surface thus including influence phenomena [17, 22–24]. Both approaches reveal similar results and succeed in describing the z-dependency of the tip-sample interaction according to the experiments but quantification is still an issue [13, 15–18, 22].

Although all of these methods are successful tools to characterize surfaces and structures, there are still open questions to be dealt with. In MFM quantitative measurements require the consideration of capacitive coupling effects based on tip-sample interaction due to V_{CPD}. Fitting data in MFM on non-magnetic nanoparticles revealed a large effective area between tip and substrate [4, 25], whereas EFM measurements with large voltages show a much smaller effective area [13]. Measuring MFM phase shifts on non-magnetic materials corresponds to EFM phase shifts for V_{DC} equals zero. Therefore, measuring the voltage parabola in EFM the vertex of the parabola images the MFM signal. Thus, investigating the voltage parabola in EFM also delivers information on the MFM tip-sample interaction.

In KPFM lateral resolution limits are still an issue [5, 26, 27]. Sorokina *et al* discussed in detail the factors influencing the accuracy. The influence of the tip state, such as the presence of defects, oxide layers and contamination, as well as the distance between tip and substrate [28]. Burnham *et al* observed a long-range interaction between the tip and sample for experiments if no voltage is applied. This group explained this effect by so-called patches, regions with different work functions [29]. Zerweck *et al* reported a change of V_{CPD} with the tip-sample distance which cannot be explained so far [5]. In KPFM and EFM, the geometry of the tip plays a crucial role in determining lateral resolution. In particular, the influence of the cantilever on the tip–substrate interaction has been examined in detail [5, 6]. Frequency-modulated KPFM is recommended to optimize lateral resolution. Polak *et al* further report that lateral accuracy can be enhanced by applying higher DC voltages [30]. In multiple publications over the last two decades a non-zero vertex is visible, yet it is rarely acknowledged [3, 8, 9, 13, 27, 31–34]. Other approaches eliminate the offset of the parabola along the y axis [35–37]. The vertex of the voltage parabola occurs where V_{DC} equals V_{CPD}, demonstrating that the non-zero vertex highlights the significant role of V_{CPD} in EFM. This must be addressed to fully explain the observed behavior.

Historically, in 1991, Nonnenmacher *et al* developed the KPFM technique using a cylindrical tip to measure V_{CPD} [38]. In their approach, V_{CPD} was added to the applied voltage, which is valid because the system was approximated as two parallel plates; the cylindrical shell does not contribute, as its surface is perpendicular to the substrate. In 1997, Hudlet *et al* developed an analytical model for AFM in which a conical tip was subdivided into cantilever, cone, and apex regions to account for their distinct geometries [17]. Using this model, Hudlet calculated the electrostatic force between the tip and the substrate. Subsequently Nonnenmacher's and Hudlet's models were combined by incorporating V CPD into Hudlet's analytical framework to calculate the electrostatic force in EFM. Thus, a parallel-plate capacitor model was applied to a conical tip geometry. The derived equation is justified under certain conditions but fails when V_{DC} approaches V_{CPD}, as this combined equation does not distinguish between the origins of the voltages—V_{CPD} simply is assumed as a small additional DC voltage and is subtracted from or added to the external voltage depending on the sign of V_{CPD} [3, 4, 15–18, 39].

In literature, dealing with analytical models there is a clear separation in the equations between the voltage contributions and the models for the tip-substrate capacitance. Apex, cone and cantilever are taken into account in the capacitance, all voltage contributions are summarized in a total voltage. But taking into account the origin of the voltages these models have to be extended. In this work this effect is discussed by a new tip substrate capacitance model named "Extended Hudlet Model". In this model for voltages comparable with V_{CPD} the cone contribution is the dominant part predicting an increase in the effective area A_{eff} approaching V_{CPD} and predicting a non-zero vertex of the voltage parabola.

In summary, so far there is no explanation as to why the effective area in MFM is larger than expected, why there are still unexplained lateral resolution limits in KPFM and why a non-zero vertex of the voltage parabola is observed in EFM measurements. The aim of these investigations is to address these open questions in experiment and theory by revisiting the concept of contact potential difference.

2. Experimental section

All AFM measurements in this paper are performed under ambient conditions (20 °C/ 50%RH) with a Dimension ICON Atomic Force Microscope from Bruker Inc. (Billerica, MA, USA) with a Nanoscope V Controller in EFM/MFM-Mode. EFM utilizes a two-scan technique: the first scan is in intermittent contact mode to get topographic information; the second scan is in non-contact mode at a defined distance to the sample (lift height) to measure electrostatic forces. The measurements are performed at a scan rate of 1 Hz with 256 samples per line. Linear and lift mode have been used. In linear mode the height above the substrate is constant and the topography of the sample is ignored. In lift mode the height above the sample topography is held constant, which means the tip follows the topography. For measurements using linear mode: The lift height is determined by adding the desired lift height above the particle z to the height of the particle d as measured by the topography scan of the AFM. The sum of particle height d and lift height above the particle z is put in the AFM as total lift height $z_1 = z + d$.

To determine the phase shift the software NanoScope Analysis 1.9 from Bruker Inc.(Billerica, MA, USA) is used. First the phase image is flattened by using the 'Flatten' tool to remove the overall phase shift caused by stray capacities. With the 'section' tool a slice across the maximum of the phase shift caused by the particle is drawn. The mean value of the signal next to the particle and the mean value of 9 data points above the center of the particle are used to determine the phase shift. The error is determined by the standard deviation of the phase signal next to the particle. This is repeated for every DC voltage and nanoparticle.

The cobalt chromium coated AFM-Probes used are SSS-MFMR from NanoSensors (Neuchatel, Switzerland). The nominal tip radius is 15 nm. The uncoated silicon AFM-probes FMR from NanoWorld AG (Neuchatel, Switzerland) have a nominal tip radius of less than 8 nm. All models have a nominal spring constant of 2.8 N m^{-1}, a nominal resonance frequency of 75 kHz. The samples are prepared by diluting the nanoparticle dispersion in ultrapure deionized water(10 µl in 10 ml) to avoid aggregation. The diluted dispersion (30 µl) is then drop casted onto a freshly cleaned 25 × 25 mm p-Si die and dried in a nitrogen atmosphere. The same is repeated for a 25 × 25 mm p-Si die with sputtered copper (200 nm, $r_q = 3$ nm) and for a 25 × 25 mm p-Si die with evaporated aluminium (100 nm, $r_q = 5$ nm). Non-functionalized polystyrene nanoparticles (100 nm, 10 mg ml^{-1}) were purchased from Alphananotech Inc. (Vancouver, Canada). The nominal tip radius cannot be used for quantitative evaluations due to wear and deformation. This is especially a problem for metal-coated tips [15]. Instead, the tip radius is calculated for each measurement based on the method by Markiewicz *et al* [40]. To measure the offset of the parabola the measurement is performed in lift mode to increase the signal-to-noise ratio (SNR). Due to the topographic effect, higher phase shifts are expected [4, 13, 41]. The measurement parameters are the same as for the investigation of the effects of DC voltage on the effective area. Two models of AFM-probes were used (SSS-MFMR; FMR). For each model the exact same tip is used to eliminate the influence of tip radii variation and other inconsistencies due to production differences.

Trapped charges can significantly affect the phase signal, for example by shifting the vertex of the voltage parabola or causing deviations from a parabolic shape [42]. Therefore, consistent V_{CPD} values obtained through KPFM indicate the absence of trapped charges. Additionally, we verified our measurements using conducting substrates. V_{DC} curves recorded with aluminum and copper substrates yielded similar results, supporting the assumption that no trapped charges were present in our experiments.

To variate V_{CPD} p-type silicon, evaporated aluminium and sputtered copper are used. The cone angles of the used AFM-probes are measured in SEM using a Supra 40 from Zeiss (Jena, Germany) at an acceleration voltage of 3 kV.

3. Theory

3.1. General considerations

In order to understand why in MFM measurements the effective area corresponding to the tip-substrate-capacitance differs from the effective area in EFM measurements at high voltages the interaction between tip and substrate in general needs to be discussed.

All theoretical approaches to date, such as analytical calculations and complex 3D simulation have been proven to fit the z-dependency of the phase shift but quantification of measurements is still an issue. All simulations so far are based on Hudlet's assumption of constant potential on the conducting surface [15, 18, 22]. Simulations are based on solving Poisson's equation for a conductive tip and a conductive substrate. The resulting potential distribution reflects influence phenomena such as the accumulation of electrons at the apex of the tip (figure 1).

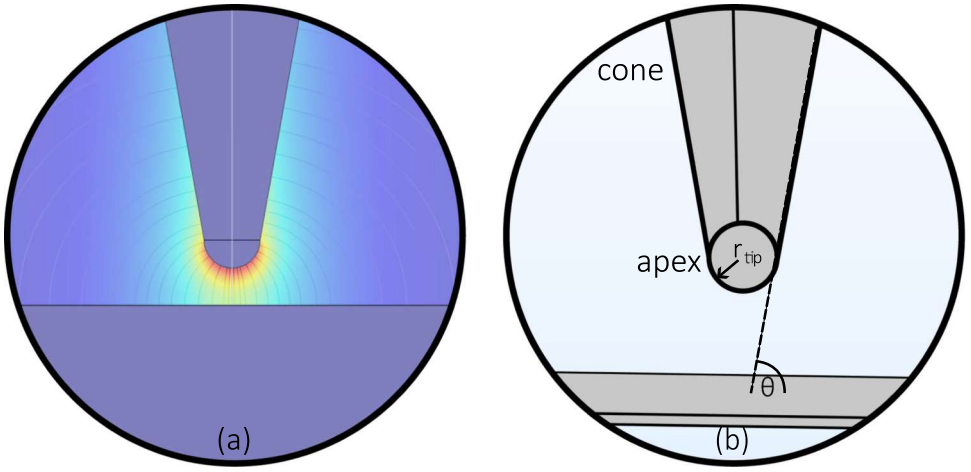

Figure 1. Equivalent models for the tip-substrate interaction: (a) Simulation: solving Poisson's equation for conducting tip and substrate(red = high and blue = low electric field strength) [23]; (b) analytical model by Hudlet [17, 18]: contribution of cantilever, cone and apex of the tip (exact tip form needed).

3.2. Considerations on the contact voltage difference in EFM, KPFM and MFM

When two different metals are brought into contact, a contact potential difference arises leading to aligned Fermi levels of both metals and an internal electric field at the interface due to separated charges. The contact potential difference is a material property which can be nullified by applying an external voltage under certain geometrical conditions. For example in KPFM the goal is to apply an external voltage V_{DC} such that it nullifies the electrostatic force due to V_{CPD}. This can be achieved for two parallel metal surfaces [7]. As soon as there are geometrical variations like in scanning probe methods, representing a system of a curved tip interacting with a flat surface, the local charge distribution is changed. The tip-cone acquires a surface charge distribution to satisfy boundary conditions including V_{CPD}. The intrinsic V_{CPD} between the two materials stays constant whereas the electric field, the capacitance and measurable forces become position-dependent, leading to a non-uniform charge distribution satisfying the electrostatic boundary conditions. Charges rearrange to maintain V_{CPD}. Applying an external voltage the contact potential difference still exists all over the tip and thus the tip cone still contributes to the signal. The tip, including its cone and apex, constitutes an equipotential surface which can be described by solving the Poisson equation.

In EFM tip and substrate form a capacitor which can be modelled as two metallic bodies not in physical contact, across which a voltage difference is applied. Applying a voltage between two such isolated metals shifts the electrostatic potential of one relative to the other. It is important to note that the contact potential difference V_{CPD} plays a fundamentally different role than the applied bias voltage V_{DC}. While V_{DC} causes a redistribution of free electrons towards the tip apex, V_{CPD} can be visualized as a homogeneous, local charge distribution on the tip surface. Thus, for voltages significantly larger than V_{CPD}, the apex becomes the dominant contributor to the phase signal in EFM. However, as V_{DC} approaches V_{CPD}, the influence of the tip cone becomes increasingly significant.

Figure 2 illustrates the distinct effects of V_{DC} and V_{CPD} in EFM. For simplicity the sign of V_{DC} and V_{CPD} are assumed to address negative charges on the tip. V_{DC} induces a concentration of free electrons at the apex, thereby restricting the interaction area between tip and substrate to the apex. In contrast V_{CPD} leads to a homogeneous local charge distribution on the tip causing the cone to dominate the interaction area. Therefore, the different origins and effects of V_{CPD} and V_{DC} must be carefully considered in EFM.

The same principle applies to KPFM. It is well known that high DC voltages reduce the interaction area between tip and substrate, whereas low DC voltages increase it, reducing lateral resolution [43]. Additionally it is reported that the cone shape design influences the lateral resolution limit in KPFM [6].

In MFM no external voltage is applied. The only voltage contributing to capacitive coupling between the tip and substrate arises from V_{CPD} between tip and substrate material, and the interaction area is defined primarily by the tip cone. Therefore, the interaction area in MFM is generally larger than in EFM when high voltages are used which is in accordance with experiments [3, 13]. These considerations can be transferred into theory by extending the analytical model by Hudlet [17].

3.3. Extending the hudlet model for EFM by differentiating voltage contribution

In the Hudlet model the electrical contribution to the signal arises from the voltage between the sample and the conducting probe according to equation (1) [17].

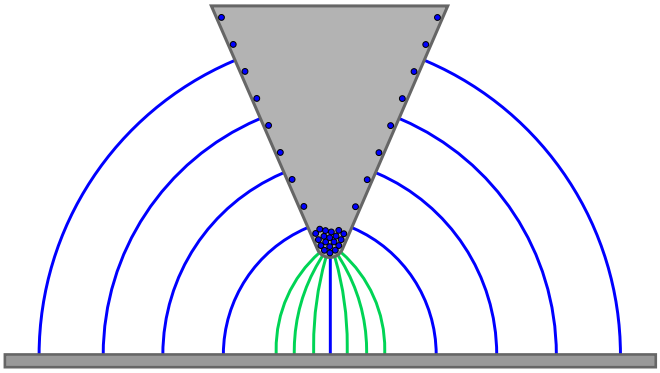

Figure 2. Schematic illustration of charge concentration at the apex of the AFM probe due to V_{DC}, leading to a reduction of the interaction area. In contrast, V_{CPD} leads to a increased interaction area due to the charge distribution on the cone surface to maintain V_{CPD}.

$$F = \frac{1}{2}\frac{dC}{dz}V_{tot}^2 \tag{1}$$

with C being the capacitance between tip and substrate, V_{tot} the total voltage between tip and substrate and z the lift height. The force gradient which acts on the tip is given by $F' = \frac{1}{2}C''V_{tot}^2$ wherein C'' denotes for the second derivative of the capacitance. The phase signal is given by equation (2).

$$\Phi_{el} = -\frac{Q}{k}F' \tag{2}$$

with the quality factor of the cantilever Q and the spring constant k.

The total voltage is composed of different contributions: the externally applied voltages V_{DC} and V_{AC}, the voltage due to the contact potential difference V_{CPD} and the voltage due to trapped charges V_Q (equation (3)) [3, 44].

$$V_{tot} = V_{DC} + V_{CPD} + V_Q + V_{AC}\sin(\Omega t) \tag{3}$$

V_{DC} and V_{AC} only occur in EFM measurements, V_{CPD} and V_Q also contribute to MFM measurements. For simplicity the absence of trapped charges is assumed ($V_Q = 0$) and $V_{AC} = 0$. The EFM tip consists of a cantilever and a conical tip including a spherical apex with radius r_{Tip}, all contributing to the capacitance between tip and substrate as in detail discussed and simulated in literature (equation (4)) [16–18, 44].

$$F = \frac{1}{2}\left(\frac{dC_{Cantilever}}{dz} + \frac{dC_{Cone}}{dz} + \frac{dC_{apex}}{dz}\right)V_{tot}^2 \tag{4}$$

In literature there is so far a clear separation in the equations between the voltage contributions and the models for the tip-substrate capacitance. All voltage contributions such as V_{DC}, V_{CPD}, V_{AC} and V_Q are added and treated in the same manner but the different origin of the voltages is neglected. But taking into account the origin of the voltages as discussed in 3.2 these models have to be extended. The origin of V_{CPD} is the difference of the electron work function between tip and substrate material. In a simple picture it can be imaged as localized charges on the complete tip surface including apex, cone and cantilever acting as a homogeneous charge distribution on the tip. However, applying an external voltage between tip and substrate using a conductive tip leads to a charge accumulation in the apex of the tip and an enhanced electric field between apex and substrate due to influence in accordance with the Poisson equation. Therefore the equations have to be adapted taking into account the origin of the voltages resulting in the Extended Hudlet Model (equation (5)). The contribution of the cantilever is small due to the large distance between cantilever and substrate in the experiments. Therefore, its contribution is neglected here in the following.

$$F = \frac{1}{2}\left(\frac{dC_{apex}}{dz}\right)(V_{DC} + V_{CPD})^2 + \frac{1}{2}\left(\frac{dC_{Cone}}{dz}\right)(V_{CPD})^2 \tag{5}$$

Respectively the phase signal corresponds to equation (6).

$$\Phi_{el} = -\frac{1}{2}\frac{Q}{k}\left[\left(\frac{d^2C_{apex}}{dz^2}\right)(V_{DC} + V_{CPD})^2 + \left(\frac{d^2C_{Cone}}{dz^2}\right)(V_{CPD})^2\right] \tag{6}$$

The first part of equation (6) delivers a parabola with contributions from the apex of the tip. The second part of the equations denotes the additional contribution of V_{CPD} of the cone to the phase signal. The contribution of apex and cone to equation (6) according to Hudlet are shown in equation S1 for the apex and equation

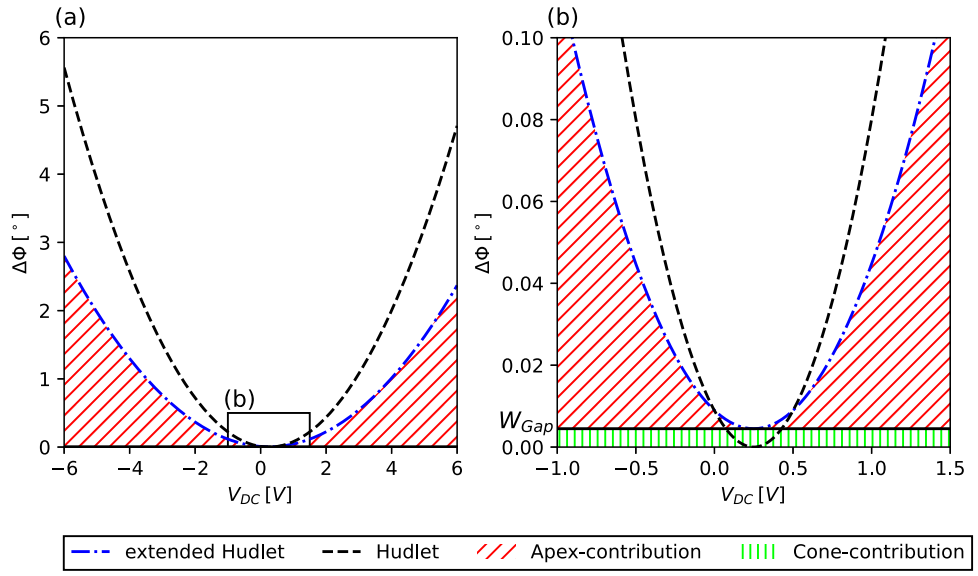

Figure 3. Using equation (6) for the Extended Hudlet Model the phase shift can be calculated ((a) from −6 to 6 V and (b) −1 to 1.5 V). The apex and cone-contribution are clearly separated in the Extended Hudlet model, leading to a shift of the parabola creating a gap between its vertex and 0° with the width W_{Gap}. In contrast, the Hudlet model does not separate the voltages at apex and cone. Therefore the parabola shows no offset.

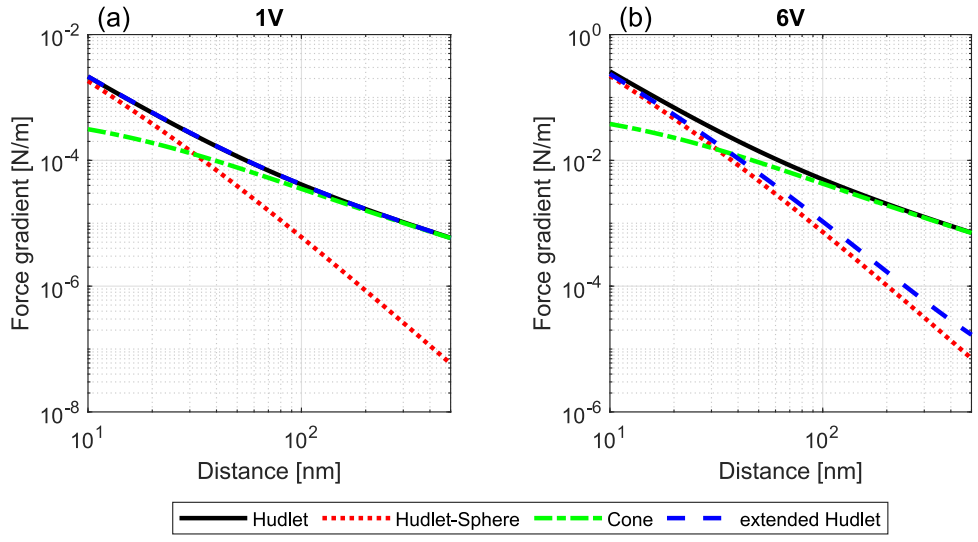

Figure 4. Calculating the force gradient as a function of tip-sample distance from 10 nm to 500 nm of Hudlet, Hudlet-Sphere, Hudlet-Cone and the Extended Hudlet Model shows a clear difference in force gradient near V_{CPD} (a) $V_{DC} = 1$ V and voltages significantly larger than V_{CPD} (b) $V_{DC} = 6$ V. V_{CPD} being 0.5 V for this calculation.

S2 for the cone in the supporting information. As the origin of V_{CPD} arises from the different electron work functions of the tip and substrate material the whole tip, both cone and apex, contributes to the electrical signal. Thus, this equation predicts a non-zero vertex of the voltage parabola in EFM indicating that even if V_{DC} equals V_{CPD} there is still a small phase signal illustrated in figure 3. For voltages much higher than V_{CPD} the first term dominates the second term and implies that the effective area of the overall tip-substrate capacitor is based on the radius of the apex and therefore independent of the distance between tip and surface.

Figure 4 presents the difference between the Hudlet, Hudlet's sphere, cone and the Extended Hudlet model for a voltage close to V_{CPD} (1V) and a voltage much larger than V_{CPD} (6V). At high voltages, in the Extended Hudlet Model, the force gradient as a function of tip–substrate distance is no longer dominated by the conical part of the tip as it is expected from the Hudlet model. Instead, in the range from 30 nm to 500 nm, a clearly dominant contribution of the apex is shown.

In summary, the Extended Hudlet Model significantly deviates from previous models if the applied voltage approaches V_{CPD} and at voltages much higher than V_{CPD}.

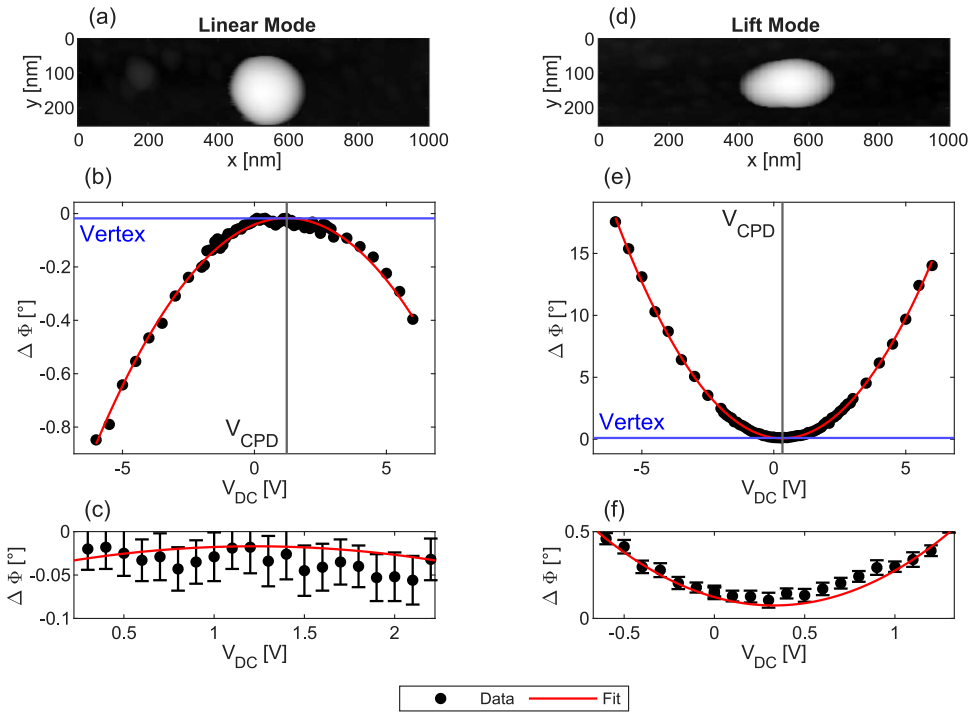

Figure 5. (a)–(c) linear mode measurement of a 126 nm PS nanoparticle (CoCr coated tip, 33 nm tip radius); (d)–(f) lift mode measurement of a 113 nm PS nanoparticle (CoCr coated tip, 46.9 nm tip radius): (a)Topographic scan; (b) Phaseshift as function of tip voltage over the nanoparticle shown in (a) in linear mode; (c) Phaseshift near V_{CPD} as function of tip voltage shown in (a); (d) Topographic scan; (e) Phaseshift as function of tip voltage over the nanoparticle shown in (d) in linear mode; (f) Phaseshift near V_{CPD} as function of tip voltage shown in (e).

Using the lift mode and measuring three dimensional nanostructures the change in distance leads to a change in capacitance beside and above the nanostructure and has to be taken into account so that the measured phase signal is given by [3, 4, 41] as described and discussed in detail by Krivcov *et al* (equation (7)) [45].

$$\Delta\Phi_{el} = -\frac{Q}{k}(F'(z+d) - F'(z)) \tag{7}$$

with z being the lift height and d the height, respectively, diameter of the nanostructure.

4. Results and discussion

The aim of this work is to experimentally investigate the tip-substrate interaction in Electrostatic Force Microscopy. The Extended Hudlet Model predicts a non-zero vertex as described in section 3.3 which is referred to as gap in the following. The vertex is defined by the extremum of the voltage parabola. The position of the vertex corresponds to V_{CPD}. The width of the gap, W_{Gap}, is expected to be proportional to the square of V_{CPD} according to the Extended Hudlet Model.

In order to demonstrate the relevance of the Extended Hudlet Model for EFM measurements dielectric nanoparticles are chosen as a model system for experiments. Using linear mode instead of lift mode suppresses topographic crosstalk resulting in the only contrast being the dielectric change when the tip is above the nanoparticle. Therefore, the interaction area of the tip-nanoparticle-substrate system is laterally restricted by the size of the nanoparticle [4].

Figures 5(a)–(c) shows linear mode measurements of a polystyrene (PS) nanoparticle with a diameter of 126 nm. The topographic scan is shown in figure 5(a). The measured height corresponds to the diameter of the particle. The corresponding phase shift as a function of voltage in linear mode is displayed in figure 5(b). As linear mode is used topographic crosstalk is suppressed. The observed phase is negative as the dielectric constant of the nanoparticle is the only contrast in linear mode measurements [4]. The measurements are done at a lift height of 50 nm. Here the lift height is defined as the distance between tip and nanoparticle. The contact potential difference V_{CPD}, determined by the position of the vertex, for the particle is −1.22 V. The measurement shows a non-zero vertex with the width of the gap, W_{Gap} of −0,017°.

The measured width of the gap and therefore the signal to noise ratio is very small. The error is in the range of ±0.025°. The main contributor to this error is the topographic crosstalk due to surface roughness of the

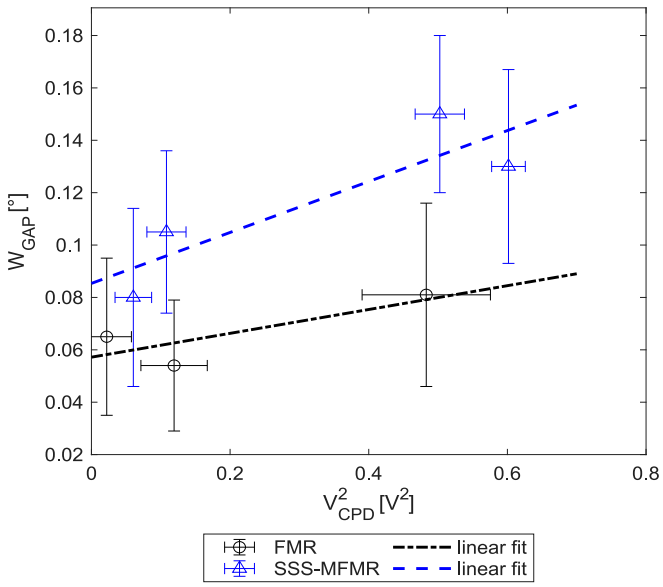

Figure 6. Phaseshift at $V_{DC} = V_{CPD}$, W_{Gap} is plotted over V_{CPD}^2 over 100 $\pm$5 nm PS-NPs on substrates with various contact potential differences to the two types of tips used [Si-tip (FMR) and CoCr-coated-tip (SSS-MFMR)]. The slope for the FMR Tips is 0.046° V_{CPD}^{-2} and for the CoCr-Tips is 0.097° V_{CPD}^{-2}.

substrate. Thus, although the non-zero vertex clearly is visible linear mode does not allow measurements of the width of the gap as a function of V_{CPD}.

Therefore, lift mode measurements (figures 5(d)–(f)) are conducted which include topographic crosstalk resulting in an increased signal to noise ratio due to the distance change between tip and substrate measuring above the nanoparticle. Thus, a comparison of particles is only possible for particles of the same diameter because in this case the contribution of topographic crosstalk is the same and therefore can be neglected. In contrast to linear mode measurements the parabola of lift mode measurements shows positive values as the distance change between tip and substrate measuring above the particle leads to a positive phase shift [3]. Due to the topographic crosstalk the width of the gap, the phase signal for $V_{DC} = V_{CPD}$, increases compared to linear mode measurements. The improved signal to noise ratio now allows to determine the dependency of the width of the gap as a function of V_{CPD}. Note: The width of the gap includes the contribution of the topographic crosstalk. Therefore, the absolute value of the gap width has no relevance and is not a measure of the value predicted in the Extended Hudlet Model.

As well the linear mode as the lift mode measurements reveal a non-zero vertex of the voltage parabola as predicted in the Extended Hudlet model. The origin of V_{CPD} can be imagined as localized charges ('pinned charges') on the complete tip surface including apex and cone. Therefore, the shape of the tip is very important and leads to a complex interaction between different parts of the tip and the substrate. Applying a DC voltage between tip and substrate leads to a charge accumulation by free charges in the apex of the tip due to influence phenomena and thus an enhanced electric field between apex and substrate according to Poisson's equation. Treating V_{CPD} similar to the applied voltage would lead to an overestimated accumulation of free charges in the tip as well as to a suppression of the effect of 'pinned charges' on the cone of the tip. V_{CPD} needs to be assumed as a constant voltage between all parts of the tip and the substrate. Thus, for V_{DC} approaching V_{CPD} the cone becomes more and more important and therefore there is no complete compensation of V_{CPD} by V_{DC} leading to a non-zero vertex of the parabola.

In order to investigate the dependence of the width of the gap on V_{CPD} the substrate material is changed. Nanoparticles on three different substrates namely p-type silicon, copper and aluminium are investigated with two different tips (Si-Tip: FMR and CoCr-coated-Tip: SSS-MFMR). The measured contact potential difference for each material combination can be found in the supporting information.

Figure 6 shows the the width of the gap, W_{Gap}, as a function of V_{CPD}^2 measured for 100 $\pm$5 nm polystyrene nanoparticles. The contact potential difference is determined by fitting an arbitrary parabola ($\Delta\Phi = a(V_{DC} - b)^2 + c$) to the measurement data, where b equals V_{CPD}. The two tips differ in size ($r_{Tip} = 23$ nm (FMR) and $r_{Tip} = 45$ nm ($SSS-MFMR$)) which explains the larger W_{Gap} for the CoCr-coated tip as a larger tip radius corresponds to an increased effective area of the capacitor due to convolution effects. W_{Gap} is increasing with V_{CPD}^2 and seems to be linearly dependent on V_{CPD}^2 but the uncertainty is too large to confirm this dependency.

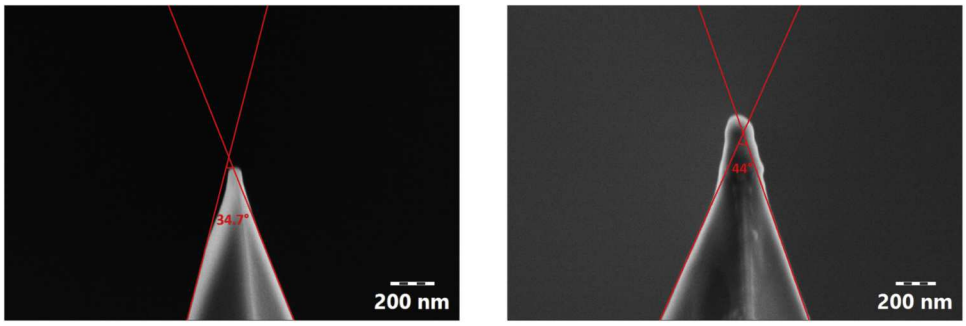

(a) FMR (b) SSS-MFMR

Figure 7. SEM images of FMR-Type AFM-probe from NanoWorld (Neuchâtel,Switzerland) and SSS-MFMR-Type AFM-probe from NANOSENSORS (Neuchâtel,Switzerland) from the front with the measured side to side angle.

The error is in the range of $\pm 0.025°$. The steeper slope of the SSS-MFMR probe is most likely due to a larger cone half angle which is confirmed by SEM measurements (figure 7). The cone angles near the tip are 34.7° for FMR and 44° for SSS-MFMR probes measured side to side. Measured from front to back the tip angles are 46° for FMR and 60° SSS-MFMR probes. More SEM images can be found in the supporting information.

The Extended Hudlet Model predicts an increasing W_{Gap} with V_{CPD}^2 which corresponds to the measurements.

As well the presence of a gap when V_{DC} equals V_{CPD} as the increase of the gap's width on V_{CPD} support the Extended Hudlet Model. These measurements demonstrate the necessity of accounting for the origin of V_{CPD} when modeling the tip–substrate interaction.

5. Conclusion

Investigations of the voltage parabola in linear mode as well as in lift mode measurements show a non-zero vertex of the parabola indicating that the voltage applied never completely compensates V_{CPD}. The width of the gap is increasing with V_{CPD}^2. This indicates an influence of V_{CPD} on W_{Gap}. To confirm this further research is needed and ongoing. Both effects, the non-zero vertex of the parabola and its increase with V_{CPD}, are based on the different origin of V_{CPD} and V_{DC}. An applied DC voltage addresses the free electrons in the conducting material of the tip leading to an accumulation of the free electrons in the apex of the tip. In contrast the effect of V_{CPD} can be described as homogeneous distributed pinned electrons on the whole tip surface. Thus, V_{CPD} and V_{DC} must be treated different in theory as well. In this paper the Extended Hudlet model, differentiating between the origin of the two voltage contributions, succeeds in explaining the observed non-zero vertex of the voltage parabola in EFM. These findings could also explain an enlarged interaction area between tip and substrate observed in MFM measurements as well as the lateral resolution limits in KPFM by enhanced cone contributions. These findings are not limited to dielectric nanoparticles and could be expanded to biological samples (e.g. bacteria and viruses). Since the shape of biological samples is often not spherical, this has to be taken into account. Furthermore, this research helps improving quantitative dielectric constant measurements or enabling better correction in KPFM imaging. In summary, this approach enables a more accurate and quantitative interpretation of MFM, KPFM, and EFM data.

Acknowledgments

The authors acknowledge the financial support by the German state Rhineland-Palatinate, the European Regional Development Fund (ERDF), through the ongoing project 'KoMBio-Hyperthermiesysteme aus superparamagnetischen Funktionsmaterialien zum kontaktlosen Heizen in Medizintechnik und Biotechnologie'.

Data availability statement

The data cannot be made publicly available upon publication because no suitable repository exists for hosting data in this field of study. The data that support the findings of this study are available upon reasonable request from the authors.

Funding

This research was funded by the European Regional Development Fund (ERDF), co-funded by the German state Rhineland-Palatinate.

Supplementary data

Supplementary material for this article is available online.

Author contributions

Lukas Lehnert 0000-0002-7522-6851
Data curation (lead), Formal analysis (lead), Methodology (lead), Software (lead), Visualization (lead), Writing – original draft (lead), Writing – review & editing (lead)

Ronald Thoelen 0000-0001-6845-0866
Supervision (supporting)

Hildegard Möbius 0000-0003-2725-9752
Conceptualization (lead), Funding acquisition (lead), Project administration (supporting), Validation (lead)

References

[1] Angeloni L, Passeri D, Reggente M, Mantovani D and Rossi M 2016 Removal of electrostatic artifacts in magnetic force microscopy by controlled magnetization of the tip: application to superparamagnetic nanoparticles *Sci. Rep.* **6** 26293
Livia Passeri A, Reggente D, Mantovani M and Rossi D 2016 Marco eng England 2016/05/20 *Sci. Rep.* **6** 26293
[2] Vokoun D, Samal S and Stachiv I 2022 Magnetic force microscopy in physics and biomedical applications *Magnetochemistry* **8** 42
[3] Krivcov A, Junkers T and Möbius H 2018 Understanding electrostatic and magnetic forces in magnetic force microscopy: towards single superparamagnetic nanoparticle resolution *J. Phys. Commun.* **2** 075019
[4] Fuhrmann M, Krivcov A, Musyanovych A, Thoelen R and Möbius H 2020 The role of nanoparticles on topographic cross-talk in electric force microscopy and magnetic force microscopy *Phys. Status Solidi A* **217** 1900828
[5] Zerweck U, Loppacher C, Otto T, Grafström S and Eng L M 2005 Accuracy and resolution limits of kelvin probe force microscopy *Phys. Rev. B* **71** 125424
[6] Sadewasser S and Glatzel T 2018 *Experimental Technique and Working Modes* (Springer International Publishing) pp 3–22
[7] Melitz W, Shen J, Kummel A C and Lee S 2011 Kelvin probe force microscopy and its application *Surf. Sci. Rep.* **66** 1–27
[8] Lilliu S, Maragliano C, Hampton M, Elliott M, Stefancich M, Chiesa M, Dahlem M S and Macdonald J E 2013 Efm data mapped into 2d images of tip-sample contact potential difference and capacitance second derivative *Sci. Rep.* **3** 3352
[9] Gkountaras A, Kim Y, Coraux J, Bouchiat V, Lisi S, Barsoum M W and Ouisse T 2020 Mechanical exfoliation of select max phases and mo(4) ce(4) al(7) c(3) single crystals to produce maxenes *Small* **16** e1905784
[10] Vogel E 2007 Technology and metrology of new electronic materials and devices *Nat. Nanotechnol.* **2** 25–32
[11] Coster H G 2003 The physics of cell membranes *J. Biol. Phys.* **29** 363–99
[12] Revilla R I 2016 Characteristic tip substrate capacitance studied using force spectroscopy method of atomic force microscopy *arXiv: Mesoscale and Nanoscale Physics*
[13] Fuhrmann M, Musyanovych A, Thoelen R and Moebius H 2022 Determination of the dielectric constant of non-planar nanostructures and single nanoparticles by electrostatic force microscopy *J. Phys. Commun.* **6** 125005
[14] Gramse G, Casuso I, Toset J, Fumagalli L and Gomila G 2009 Quantitative dielectric constant measurement of thin films by dc electrostatic force microscopy *Nanotechnology* **20** 395702
[15] Fumagalli L, Esteban-Ferrer D, Cuervo A, Carrascosa J L and Gomila G 2012 Label-free identification of single dielectric nanoparticles and viruses with ultraweak polarization forces *Nat. Mater.* **11** 808–16
[16] Belaidi S, Girard P and Leveque G 1997 Electrostatic forces acting on the tip in atomic force microscopy: Modelization and comparison with analytic expressions *J. Appl. Phys. (Melville, NY, U. S.)* **81** 1023–30
[17] Hudlet S, Saint Jean M, Guthmann C and Berger J 1998 Evaluation of the capacitive force between an atomic force microscopy tip and a metallic surface *Eur. Phys. J. B* **2** 5–10
[18] Law B M and Rieutord F 2002 Electrostatic forces in atomic force microscopy *Phys. Rev. B* **66**
[19] Staii C, Johnson A T and Pinto N J 2004 Quantitative analysis of scanning conductance microscopy *Nano Lett.* **4** 859–62
[20] Guriyanova S, Golovko D S and Bonaccurso E 2010 Cantilever contribution to the total electrostatic force measured with the atomic force microscope *Meas. Sci. Technol.* **21**
[21] Gil A, Colchero J, Gómez-Herrero J and Baró A M 2003 Electrostatic force gradient signal: resolution enhancement in electrostatic force microscopy and improved kelvin probe microscopy *Nanotechnology* **14** 332–40
[22] Stan G 2023 Dielectric constant measurement sensitivity in electrostatic force and force gradient microscopy-based modes *J. Appl. Phys.(Melville, NY, U. S.)* **134**
[23] Boularas A, Baudoin F, Teyssèdre G, villeneuve faure C and Clain S 2014 3D modelling of electrostatic force distance curve between the AFM probe and dielectric surface
[24] Gomila G, Gramse G and Fumagalli L 2014 Finite-size effects and analytical modeling of electrostatic force microscopy applied to dielectric films *Nanotechnology* **25** 255702

[25] Krivcov A, Schneider J, Junkers T and Möbius H 2018 Magnetic force microscopy of in a polymer matrix embedded single magnetic nanoparticles *Phys. Status Solidi A* **216**
[26] Kaja K *et al* 2009 Effects of experimental parameters on the work function measurement: a kelvin force microscopy study
[27] Brouillard M, Bercu N, Zschieschang U, Simonetti O, Mittapalli R, Klauk H and Giraudet L 2022 Experimental determination of the lateral resolution of surface electric potential measurements by kelvin probe force microscopy using biased electrodes separated by a nanoscale gap and application to thin-film transistors *Nanoscale Adv.* **4** 2018–28
[28] Sorokina K L and Tolstikhina A L 2004 Atomic force microscopy modified for studying electric properties of thin films and crystals. review *Crystallogr. Rep.* **49** 476–99
[29] Burnham N A, Colton R J and Pollock H M 1992 Work-function anisotropies as an origin of long-range surface forces *Phys. Rev. Lett.* **69** 144–7
[30] Polak L and Wijngaarden R J 2016 Two competing interpretations of kelvin probe force microscopy on semiconductors put to test *Phys. Rev. B* **93**
[31] Riedel C, Arinero R, Tordjeman P, Ramonda M, Lévêque G, Schwartz G A, Oteyza D G, Alegria A and Colmenero J 2009 Determination of the nanoscale dielectric constant by means of a double pass method using electrostatic force microscopy *J. Appl. Phys.* **106**
[32] Patel S, Petty C W, Krafcik K, Loyola B, O'Bryan G and Friddle R W 2016 Imaging latex-carbon nanotube composites by subsurface electrostatic force microscopy *Nanotechnology* **27** 415705
[33] Pandey M, Soni R, Mathur A, Singh A, Singh A K, Raghavan S and Chandni U 2019 Noninvasive subsurface electrical probe for encapsulated layers in van der waals heterostructures *Physical Review Applied* **12**
[34] Collins L, Belianinov A, Somnath S, Balke N, Kalinin S V and Jesse S 2016 Full data acquisition in kelvin probe force microscopy: Mapping dynamic electric phenomena in real space *Sci. Rep.* **6** 30557
Liam Belianinov C, Somnath A, Balke S, Kalinin N and Jesse S V 2016 Stephen eng Research Support, U.S. Gov't, Non-P.H.S. England 2016/08/16 *Sci. Rep.* **6** 30557
[35] Gupta S, Williams O A and Bohannan E 2011 Electrostatic force microscopy studies of boron-doped diamond films *J. Mater. Res.* **22** 3014–28
[36] Lei C H, Das A, Elliott M and Macdonald J E 2004 Quantitative electrostatic force microscopy-phase measurements *Nanotechnology* **15** 627–34
[37] Shen Y, Wang Y, Zhou Y, Hai C, Hu J and Zhang Y 2018 Electrostatic force spectroscopy revealing the degree of reduction of individual graphene oxide sheets *Beilstein J. Nanotechnol.* **9** 1146–55
Yue Wang S, Zhou Y, Hai Y, Hu C, Zhang J and Germany Y 2018 *2018/05/03 Beilstein J. Nanotechnol.* **9** 1146–55 eCollection 2018
[38] Nonnenmacher M, O'Boyle M P and Wickramasinghe H K 06 1991 Kelvin probe force microscopy *Appl. Phys. Lett.* **58** 2921–3
[39] Fuhrmann M, Musyanovych A, Thoelen R, von Bomhard S and Mobius H 2020 Magnetic imaging of encapsulated superparamagnetic nanoparticles by data fusion of magnetic force microscopy and atomic force microscopy signals for correction of topographic crosstalk *Nanomaterials* **10** 2486
[40] Markiewicz P and Goh M C 1994 Atomic force microscopy probe tip visualization and improvement of images using a simple deconvolution procedure *Langmuir* **10** 5–7
[41] Van Der Hofstadt M, Fabregas R, Biagi M C, Fumagalli L and Gomila G 2016 Nanoscale dielectric microscopy of non-planar samples by lift-mode electrostatic force microscopy *Nanotechnology* **27** 405706
[42] Yang J, Kim J, Lee J, Min S, Kim H, Wang K L and Hong J 2008 Electrostatic force microscopy measurements of charge trapping behavior of au nanoparticles embedded in metal–insulator–semiconductor structure *Ultramicroscopy* **108** 1215–9
[43] Örnek C, Leygraf C and Pan J 2019 On the volta potential measured by skpfm—fundamental and practical aspects with relevance to corrosion science *Corrosion Engineering, Science and Technology* **54** 185–98
[44] Paul G 2001 Electrostatic force microscopy: principles and some applications to semiconductors *Nanotechnology* **12** 485
[45] Krivcov A, Ehrler J, Fuhrmann M, Junkers T and Mobius H 2019 Influence of dielectric layer thickness and roughness on topographic effects in magnetic force microscopy *Beilstein J. Nanotechnol.* **10** 1056–64